

# Sparse Time-Frequency Representation for Incipient Fault Diagnosis of Wind Turbine Drive Train

Boyan Yang, *Graduate Student Member, IEEE*, Ruonan Liu, and Xuefeng Chen<sup>ID</sup>

**Abstract**—As wind power attracts increasing attention and wind turbines (WTs) capacity expands, fault diagnosis of WT is playing a more and more important role in improving reliability, minimizing down time, reducing maintenance costs, and providing reliable power generation. In this paper, a novel sparse time-frequency representation (STFR) method is proposed to increase the diagnostic precision of incipient faults. The proposed method can be applied once the condition is detected as abnormal according to the VDI3834 vibration threshold standard in WT fault diagnosis systems. The proposed method is a novel signal representation method based on the sparse representation theory and Wigner–Ville distribution (WVD), which can overcome the limitations of traditional basis functions expansion and time-frequency analysis methods. In this method, a union of redundant dictionary (URD) is constructed on the basis of the underlying prior information of the oscillate characteristics with multicomponent coupling effect and different morphological waveforms. Therefore, the vibration signal can be sparsely represented over the URD. Then, the sparse coefficients and corresponding atoms can be obtained by solving the basis pursuit denoising problem via alternating direction method of multipliers. Based on the combination of the WVD of each atom and corresponding sparse coefficient, the time-frequency distribution of the vibration signal can be obtained. To verify the effectiveness of the STFR method, a simulation and two field tests in the wind farm are performed. The comparison results with state-of-the-art methods illustrate the superiority and robustness of the proposed method in the engineering applications.

**Index Terms**—Fault diagnosis, sparse representation, time-frequency representation, union of redundant dictionary (URD), wind turbine (WT).

## I. INTRODUCTION

SINCE the world energy crisis in the 1970s, the fast consumption of conventional energy sources and today's continuously increasing energy demand have necessitated intensive research for more efficient and green energy sources. Alternative energy resources such as wind, solar, ocean thermal, and tidal energy have attracted the increasing attention

Manuscript received June 28, 2017; revised January 15, 2018; accepted March 19, 2018. Date of publication May 21, 2018; date of current version October 9, 2018. This work was supported in part by the National Natural Science Foundation of China under Grant 51421004 and Grant 51605365 and in part by the National Key Basic Research Program of China under Grant 2015CB057400. The Associate Editor coordinating the review process was Dr. Eduardo Cabal-Yepez. (*Corresponding author: Xuefeng Chen*.)

The authors are with the State Key Laboratory for Manufacturing Systems Engineering, Xi'an Jiaotong University, Xi'an 710049, China (e-mail: yangboyuanxjtu@163.com; liuruonan0914@stu.xjtu.edu.cn; chenxf@mail.xjtu.edu.cn).

Color versions of one or more of the figures in this paper are available online at <http://ieeexplore.ieee.org>.

Digital Object Identifier 10.1109/TIM.2018.2828739

to generate power on a large scale [1]. Compared with fossil fuels, they are promised well to be the practical resources for modern industrial society due to their high energy density, transportability, versatility, and reasonable cost [2]. Among the main options being studied, wind farms and their constituent turbines are becoming larger and larger because of its features of environmental friendly energy, immense resources, technology maturity, good infrastructure and relative cost competitiveness, and increasing importance in the recent years [3], [4].

The worldwide total installed capacity of wind turbine (WT) from 2001 to 2014 is shown in Fig. 1(a) [5]. Meanwhile, the dramatic growth of total installation and individual capacity makes the failures of WTs costly or even unacceptable. Up to May 31, 2015, the statistics of WT accidents of the past two decades in Caithness windfarm is shown in Fig. 1(b). It can be found from the recorded data that the occurrence of accident is increasing with the growth of WTs. The failures of WTs cause not only unexpected problems of the power system because of sudden absence of a large amount of power but also high cost for repairing and maintenance, especially for those large and remote located WTs, which led to reduction in energy production [6]. Therefore, fault diagnosis has attracted increasing attention in WT applications, which is considered as an efficient way to ensure the safe running of WTs, prevent costly system maintenances, and increase productivity [7].

A WT is a complex electromechanical system with hundreds of components and subsystems [8], such as gearbox, generator, bearings, rotor hub, blades, shafts, etc. Each component of the WT has its own failure modes and contribution to the downtime. Fig. 2 shows the failure rate of major WT subsystems and the average downtime caused by the failures of these subsystems from two large surveys of onshore European WTs over 13 years [9]. From Fig. 2, it can be seen that the higher costs related to field repair and service of WTs are accredited to the drive train [10], [11]. The main structure and subsystems of a doubly fed induction generator (DFIG) WT are shown in Fig. 3. The drive train in a WT mainly consists of main shaft, gearbox, mechanical brake, and generator, as shown in Fig. 3. Therefore, in order to improve security, minimize down time, lower the frequency of sudden breakdowns, and provide reliable power generation, fault diagnosis of WT, especially the drive train, has become essential in WT applications and wind energy promotion [12].

The most important components of the fault diagnosis system are the signal acquisition and processing methods [13].

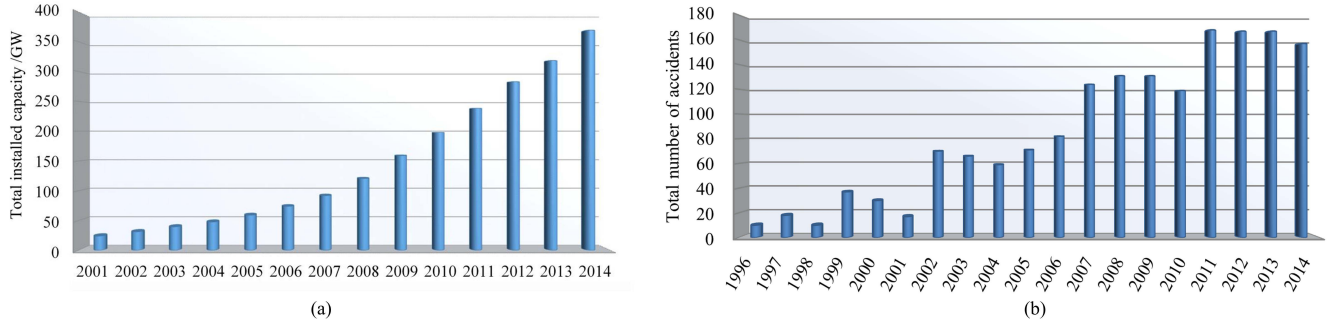


Fig. 1. (a) Worldwide WT total installed capacity from 2001 to 2014. (b) Summary of WT accidents in Caithness windfarm from 1996 to 2014.

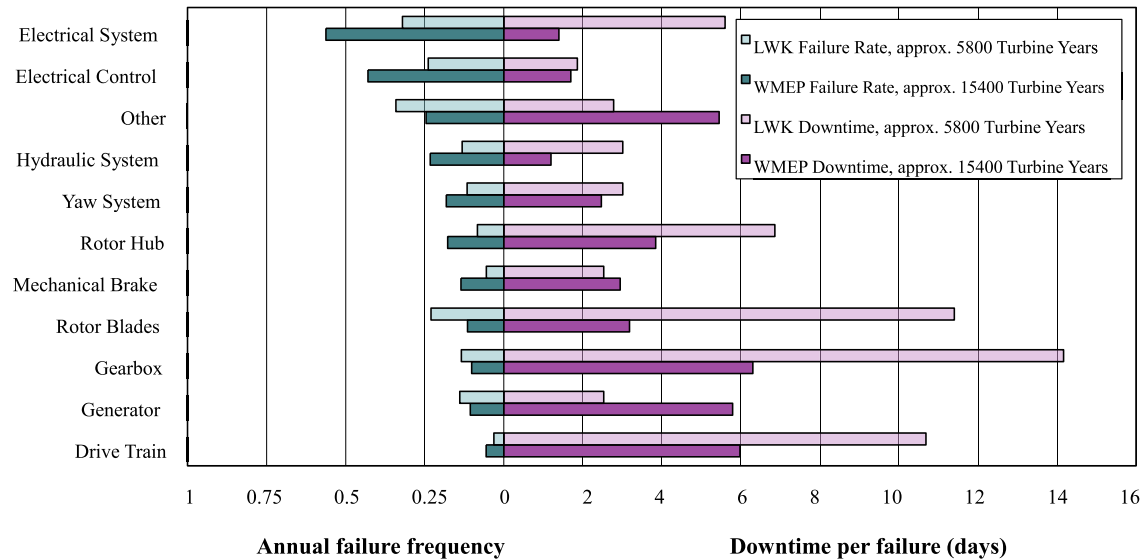


Fig. 2. Failure rate of major WT subsystems and corresponding downtime of onshore European WTs over 13 years.

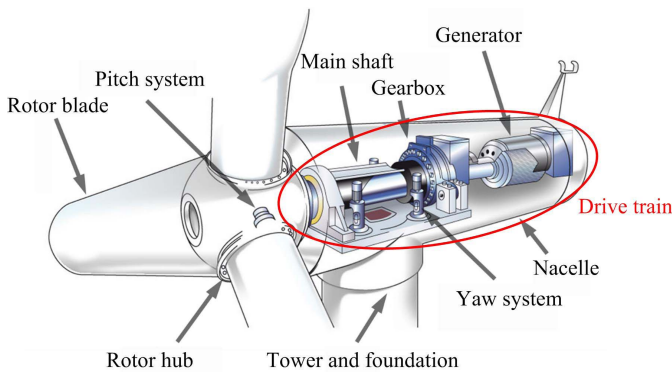


Fig. 3. Typical DFIG WT with main subsystems.

Vibration signal, strain, lubrication parameters, temperature, and acoustic emission signal are commonly used for incipient fault diagnosis [14]. They can be acquired via corresponding sensors installed in different positions of the WT. However, the measured signals are always complex and nonstationary with a large amount of background noise, and the useful information is usually too weak to be distinguished. Numerous techniques and algorithms have been proposed to deal with

this problem [15], including time-domain analysis, frequency analysis, and time-frequency analysis, such as Fourier transform [16], wavelet transform [17], [18], empirical mode decomposition [19]–[21], and spectral kurtosis [22]. These methods can partition the time-frequency position, design innumerable linear time-frequency representation methods according to the requirements, select the best band, and discover the presence of non-Gaussian signals. However, there are some drawbacks of traditional methods which are based on basis functions, such as energy leak, monotonous form, and information scatter. Recently, sparse representation of signals over various parameterized basis functions library, called the redundant dictionary, is proposed to express the complicate signals more effectively [23]–[25]. The philosophy of sparse representation theory is to concentrate the energy of feature information on a few elements and model signals as sparse linear combinations of atoms from a dictionary [26], [27]. There are mainly two well-known methods for sparse representation: matching pursuit algorithm which is proposed by Mallat and Zhang [28] and basis pursuit (BP) algorithm which is proposed by Donoho [29], [30]. Over the past several years, it has received increasing attention in signal and image processing.

In an actual engineering application, the above-mentioned state-of-the-art signal analysis techniques mainly suffer from four drawbacks: first, the signal processing effectiveness will often be weakened by the strong harmonic interferences and input noise; second, due to the coupling effect, it is difficult for the traditional methods to distinguish different faults, even health status; third, the analysis results are directly influenced by the base functions because the signals can be analyzed very well only on the condition that the time-frequency structure of signal and base function are similar, and it is often difficult to choose base functions properly in practice; last but not least, random fluctuation of wind speed will lead to WT unstable operation, which will influence the performance of diagnosis methods.

To avoid these problems, a sparse time-frequency representation (STFR) method is proposed in this paper based on sparse representation theory and the principle of time-frequency analysis. First, the evolution of the dictionary depends on how similar its base functions and the signal characteristics are, which will influence the effect of sparse representation significantly. In this method, a union of redundant dictionary (URD), which consists of two subdictionaries, is constructed based on the adequate use of the prior information on signal oscillation characteristics. Therefore, this URD can implement sparse representation of different morphological components when the WT drive train has multiple faults. Since the proposed method in this paper constructed a URD for different vibration components based on the vibration mechanism of WT driven train system, the proposed method is more pertinent and shows better resolutions. Then, the sparse coefficients of the signal after noise reduction can be obtained by solving the BP denoising (BPDN) model. The minimization problem of  $l_1$  norm in BPDN model can be transformed into a convex optimization formulation that could be dealt with the alternating direction method of multipliers (ADMM) [31]. In this paper, the vibration signal is used to analyze because it is considered as one of the optimal signals, and vibration monitoring can be found in almost all commercially available WT due to its widespread distribution and accuracy [32]. After solving the sparse model, original signal can be represented with the atoms and corresponding coefficients. Then, Wigner–Ville distribution (WVD) is used to obtain the time–frequency distribution of each atom due to their superiority in nonstationary signal processing. Finally, time–frequency distribution of original vibration signal after denoising can be represented via combining the time–frequency distribution of each atom and corresponding coefficient.

The STFR method has four main advantages: first, heavy background noise can be alleviated according to the denoising algorithm; second, compared with traditional basis function expansion methods, it can provide a better approximation to the complex signal with multicomponents coupling effect; third, the cross-term problem of the WVD can be solved by STFR; finally, it can implement the visualization of WT system condition and make the incipient fault diagnosis process more intuitive.

This paper is organized as follows. In Section II, the oscillation characteristics of WT drive train vibration signal are

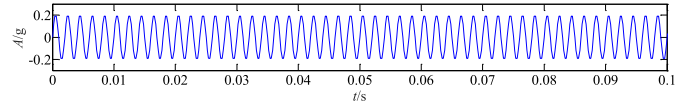


Fig. 4. Vibration signal of a normal drive train.

provided. Section III provides a detailed description of the proposed STFR method and the construction of the URD. The simulation applications are represented in Section IV. In Section V, the vibration signal analysis of two applications in WT drive trains are performed to illustrate the effectiveness of the STFR method. Finally, conclusion and future work of the research are drawn in Section VI.

## II. VIBRATION SIGNAL MODEL OF WT DRIVE TRAIN

Vibration data is recognized as the best parameter in a WT for incipient fault diagnosis during the operation, because it can reflect operational condition and faults properties rapidly, accurately, and comprehensively. There are mainly four components in the drive train vibration signal, which couple with each other and make the diagnosis even more difficult.

### A. Harmonic Component

Even in a normal WT drive train, vibration will still exist during the operation due to the fluctuation of rotating system stiffness. The waveform of vibration signal  $x(t)$  can be approximately presented as the sine wave as shown in Fig. 4.

Therefore, this component vibration signal can be described as

$$y_n(t) = \sum_{m=0}^M x_m \cos(2\pi m f_z t + \phi_m) \quad (1)$$

where  $x_m$  and  $\phi_m$  are the amplitude and phase of the  $m$ th stiffness fluctuation frequency component, respectively, and  $f_z$  is the stiffness fluctuation frequency. Specifically, stiffness fluctuation frequency represents the meshing frequency, ball passing frequency, and rotating frequency, respectively, in gearbox, shaft, and generator.

This harmonic component of vibration will always exist in either health or abnormal condition with different vibration amplitude. Therefore, it makes sense to diagnose fault based on the meshing frequency and its harmonics. However, this is not enough because the vibration signal can be influenced by faults on many aspects, such as steady modulation and impact modulation, which will be illustrated in Section II-B.

### B. Steady Modulation Component

When distributed fault occurs in a WT drive train, the vibration waveform will be modulated steadily due to the change of rotating vibration amplitude as shown in Fig. 5, which consists of harmonic component and steady modulation component.

The steady modulation model can be described as

$$y_s(t) = \sum_{m=0}^M x_m a_m(t) \cos(2\pi m f_z t + \phi_m) \quad (2)$$

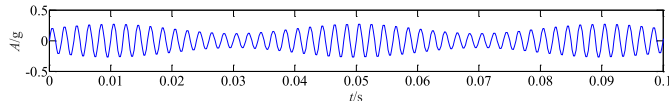


Fig. 5. Vibration waveform of a distributed fault.

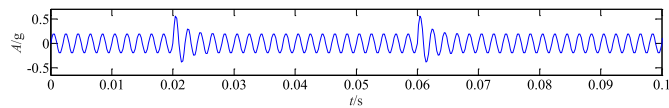


Fig. 6. Vibration waveform of a localized fault.

where  $a_m(t)$  is the  $m$ th harmonic component of the amplitude modulation, which can be modeled as

$$a_m(t) = \sum_{k=0}^N A_{m,k} \cos(2\pi k f_r t + \alpha_{m,k}) \quad (3)$$

where  $A_{m,k}$  and  $\alpha_{m,k}$  are the  $k$ th order amplitude and phase of the  $m$ th harmonic component of amplitude modulation, respectively, and  $f_r$  is the rotational frequency of the faulty unit. The carrier frequencies of steady modulation vibration signal are stiffness fluctuation frequency  $f_z$  and its harmonics, as well as modulation side-bands of rotational frequency  $f_r$  and its harmonics.

### C. Pulsing Modulation Component

In a drive train, when the rotating component passing through the defect area, the localized faults such as pitting, spall, or tooth breakage will generate impact force. The vibration signal caused by localized faults is a damped oscillation signal for which the amplitude attenuates exponentially, as shown in Fig. 6, which consists of the pulsing modulation component and harmonic component.

The model of pulsing modulation component can be described as

$$x_p(t) = A_p \exp(-2\pi \zeta / \sqrt{1 - \zeta^2} f_d t) \cos(2\pi f_d t) \quad (4)$$

where  $A_p$  is the amplitude.  $\zeta$  is the relative damping ratio.  $f_d$  is the damped natural frequency.

During the operation of a WT, rotating unit will pass the defect continuously. As a result, pulsing modulation component will occur periodically, which can be described as

$$y_p(t) = \sum_{k=-\infty}^{\infty} x_p(t - kT_n) \quad (5)$$

where  $T_n$  is the period of impacts and  $T_n = 1/f_n$  if there is only one defect.

Therefore, when the WT system is faulty, both the steady frequency modulation and the impact frequency modulation will exist in vibration signals. Even when the WT is normal, many factors will contribute to distributed faults, such as profile error, misalignment, double-elastic supporting, etc. Therefore, steady modulation component will exist in either healthy or faulty drive train.

### D. Observed Vibration Signal

As a result of the combination of above-mentioned components, the observed vibration signal of a WT drive train often can be described as

$$s(t) = y(t) + n(t) \quad (6)$$

where  $n(t)$  is the noise.  $y(t)$  is the combination signal of each components with fault information

$$y(t) = y_n(t) + y_s(t) + y_p(t) \quad (7)$$

where  $y_n(t)$  is the harmonic component.  $y_s(t)$  is the steady modulation component.  $y_p(t)$  is the pulsing modulation component.

These vibration components are often distorted by relatively strong noises, which may arise due to sensor imperfection, poor running environment or communication errors, and so on. As different components existing in the vibration signal with strong background noise, the demodulation result solved by the traditional method is always  $f_n$ , which will lead to two problems: first, it is hard to distinguish the working or faulty condition; second, it can be easily confused with distributed faults and localized faults. Furthermore, due to fluctuation of wind speed, the unsteady operation makes fault diagnosis of WT even more difficult.

Generally, the vibration signals of normal gearbox without elastic support are composed of harmonic component and noise. In this condition, for a gearbox with local fault, its vibration signals will be composed of harmonic component, pulsing modulation component, and noise. This will cause the sideband in spectrum, and characteristic frequency in their envelop spectrum, which is equal to the rotation frequency. Therefore, traditionally, the envelop spectrum and frequency spectrum are used to recognize the pulsing modulation component. However, gearboxes in WTs are usually on elastic support, which may cause the inherent misalignment, even in a normal gearbox. As a result, the vibration signals of gearboxes in WR are composed of harmonic component, steady modulation component, and noise. These components can also cause the sideband in spectrum and characteristic frequency in envelop spectrum, which makes it more difficult to diagnosis local fault in WT.

Therefore, it is necessary to work out a feature extraction algorithm of noise, steady, and pulsing coupling modulation components in nonstationary operation condition for WT incipient fault diagnosis.

## III. SPARSE TIME-FREQUENCY REPRESENTATION METHOD

### A. Basis Pursuit Denoising

The main idea of sparse representation is to replace the basis function sets with over completed redundant function sets, which are called the over completed dictionaries, and then, trace the parameterized functions matched with the signal structure features; finally, signal was represented as a linear combination of few vectors which are called atoms in the dictionary. Therefore, in sparse representation theory,

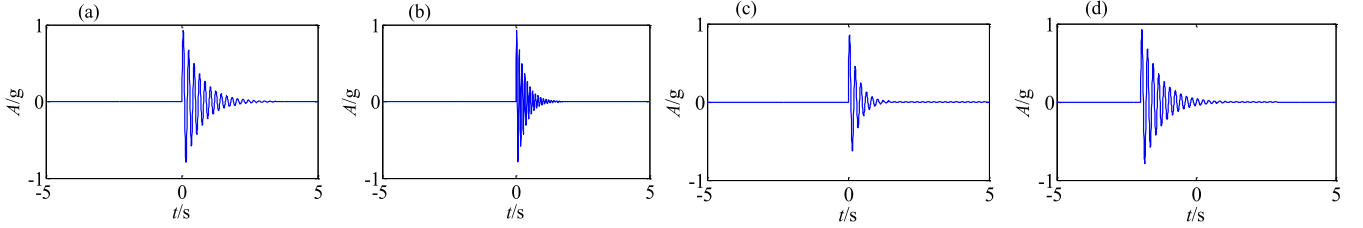


Fig. 7. Waveforms of the atoms with (a)  $\xi = 0.05$ ,  $f = 5$ , and  $\tau = 0$ , (b)  $\xi = 0.1$ ,  $f = 5$ , and  $\tau = 0$ , (c)  $\xi = 0.05$ ,  $f = 10$ , and  $\tau = 0$ , and (d)  $\xi = 0.05$ ,  $f = 5$ , and  $\tau = 2$ .

the sparser the decomposition results, the more the similarity between atoms and the nature of signal.

For the vibration signal in (7), it can be expressed as

$$\mathbf{y} = \mathbf{D}\mathbf{x}. \quad (8)$$

Let  $M$  is the length of  $\mathbf{y}$  and  $N$  is the length of  $\mathbf{x}$ . Define  $\mathbf{D}$  is an  $M \times N$  matrix, which is called the dictionary. Then, the noisy vibration signal can be rewritten as

$$\mathbf{s} = \mathbf{y} + \mathbf{n} = \mathbf{D}\mathbf{x} + \mathbf{n}. \quad (9)$$

Sparse representation of the vibration signal  $\mathbf{y}$  over the dictionary can be equivalent to an optimization problem as follows:

$$\arg \min_{\mathbf{x}} \|\mathbf{x}\|_0 \text{ s.t. } \mathbf{y} = \mathbf{D}\mathbf{x} \quad (10)$$

where  $\|\cdot\|_0$  denotes the nonzero entries of a vector. The problem in (10) is an NP-hard problem and cannot be solved in a straightforward approach. BP algorithm, proposed by Chen and Donoho, can solve the problem in (10) by replacing with  $l_1$  norm  $\|\cdot\|_1$  as the sparseness metric function. As a result, (10) can be transformed as

$$\arg \min_{\mathbf{x}} \|\mathbf{x}\|_1 \text{ s.t. } \mathbf{y} = \mathbf{D}\mathbf{x}. \quad (11)$$

For the noisy vibration signal  $\mathbf{s}$ , an approximate solution can be found by minimizing the cost function

$$\arg \min_{\mathbf{x}} \|\mathbf{s} - \mathbf{D}\mathbf{x}\|_2^2 + \lambda \|\mathbf{x}\|_1. \quad (12)$$

Parameter  $\lambda$  is the penalty factor, and should be chosen depending on the operating condition, which is usually set between 0 and 1. The larger it is, the more weight  $\mathbf{x}$  is. The problem in (12) is known as the BPDN problem. This modification leads to the conversion of the optimization problem. Because  $l_1$  norm is either a convex function or a nonstrictly concave function, the result of (12) is able to sparse represent the original signal. In this paper, ADMM method is employed to solve (12).

### B. Construction of the Union of Redundant Dictionary

In sparse decomposition method, the selection of atom dictionary is important because the sparse expression result of original signal is directly influenced by the dictionary. In order to get a better performance, the dictionary should be matched with signals inner structure as closely as possible. Therefore, the signal will be represented with less atoms and the result will be sparser. According to the vibration signal characteristic of WT drive train in Section II, this paper adequately exploits

the prior information of faulty vibration signal, and constructs a URD with two subdictionaries.

For harmonic component and steady modulation component, the vibration signal is a series of harmonic or steady modulation harmonic functions. The aim of sparse representing these two components is to find their frequencies. Therefore, frequency dictionary, which takes frequency as parameter variable, is more suitable. Fourier dictionary is a typical frequency dictionary constructed by a collection of trigonometric functions and is adapted as the first subdictionary for these two components signal.

The atom  $g_s$  of Fourier subdictionary is represented by trigonometric function with parameter  $\gamma = (f, v)$ .  $f$  is the frequency parameter.  $v \in \{0, 1\}$  is the phase parameter. When  $v = 0$  or  $v = 1$ , the waveform function is cosine or sine function, respectively

$$\begin{aligned} g_s(f, 0) &= \cos(2\pi ft) \\ g_s(f, 1) &= \sin(2\pi ft). \end{aligned} \quad (13)$$

Let  $f = k/M$ . For cosine function,  $k = 0, 1, \dots, M/2$ ; for sine function,  $k = 1, 2, \dots, M/2 - 1$ .

For pulsing modulation component, the vibration signal is a series of periodic impulse functions. Laplace wavelet, which is the spiral attenuation wave in complex number space, is very similar to free damping response function, and can represent the true vibration state of faulty drive train satisfactorily [33]. Furthermore, it has a clear physical meaning. Therefore, the atom  $g_p$  of the second subdictionary for pulsing modulation component is defined as Laplace wavelet atoms with the parameters of  $\tau$ ,  $f$ , and  $\xi$

$$g_p(\xi, f, \tau, t) = \begin{cases} Ae^{\frac{\xi}{\sqrt{1-\xi^2}}2\pi f(t-\tau)} \sin(2\pi(t-\tau)), & t \geq \tau; \\ 0, & t < \tau \end{cases} \quad (14)$$

where  $\gamma = (\xi, f, \tau)$  is the parameter vector.  $\xi$  is the damping coefficient.  $f$  is the frequency of the atom.  $\tau$  is the initial moments of pulsing response. The waveform will decrease faster as  $\xi$  increases with other parameter unaltered. When  $f$  increases with other parameter unaltered, the waveform will oscillate more rapidly.  $\xi$  and  $f$  vary from different atoms. The waveform will be translated as  $\tau$  changes.  $A$  is used for atom function normalization. The waveforms vary from different  $\tau$ ,  $f$ , and  $\xi$ , as shown in Fig. 7.

The URD is composed of the atoms in Fourier subdictionary  $g_s$  and the atoms in Laplace wavelet subdictionary  $g_p$ .

### C. Time–Frequency Representation Based on Sparse Representation and Wigner–Ville Distribution

After solving the convex optimization problem in (12) over the constructed URD, the sparse coefficients  $\hat{x}$  can be obtained. And the sum signal can be represented as

$$s(t) = \mathbf{D}\mathbf{x} = \sum_{i=1}^N \hat{x}_i g_i. \quad (15)$$

Due to the nonstationary characteristic of WT vibration signal, WVD, which is an important theoretical tool for nonstationary signal, is employed for the atom time–frequency distribution. As one of the most basic methods of Cohen bilinear time–frequency distribution, the essence of WVD is to distribute the signal energy in time–frequency plane. For signal  $s$ , the WVD is defined as

$$\mathbf{W}_s(t, f) = \int_{-\infty}^{\infty} s\left(t + \frac{\tau}{2}\right) s^*\left(t - \frac{\tau}{2}\right) e^{-j2\pi f t}. \quad (16)$$

Although WVD shows superb time–frequency concentration, the essence of its distribution is not linear, i.e., the WVD of the sum signal is not equal to the sum WVD of each signal. Let  $s(t) = s_1(t) + s_2(t)$

$$\begin{aligned} & \mathbf{W}_s(t, f) \\ &= \int_{-\infty}^{\infty} \left[ s_1\left(t + \frac{\tau}{2}\right) + s_2\left(t + \frac{\tau}{2}\right) \right] \cdot \left[ s_1^*\left(t - \frac{\tau}{2}\right) \right. \\ &\quad \left. + s_2^*\left(t - \frac{\tau}{2}\right) \right] \times e^{-j2\pi f t} = \mathbf{W}_{s_1}(t, f) + \mathbf{W}_{s_2}(t, f) \\ &\quad + 2\mathbf{Re}[\mathbf{W}_{s_1, s_2}(t, f)]. \end{aligned} \quad (17)$$

The term  $2\mathbf{Re}[\mathbf{W}_{s_1, s_2}(t, f)]$  is the mutual WVD, which is an introduced interference and known as the cross term. It is obvious that the more the components, the more the cross terms. For a signal containing  $n$  components, there will be  $C_n^2$  cross terms. For the sparse represented signal  $s$  in (15), the WVD will be

$$\begin{aligned} \mathbf{WVD}_s(t, f) &= \sum_{i=1}^N \mathbf{WVD}_{\hat{x}_i g_i}(t, f) \\ &\quad + \sum_{i=1}^N \sum_{j=1, j \neq i}^N \mathbf{Re}[\mathbf{WVD}_{\hat{x}_i g_i, \hat{x}_j g_j}(t, f)]. \end{aligned} \quad (18)$$

The second term in (18) is the cross term, which can interfere the time–frequency distribution greatly, and depress the promotion of quadratic time–frequency distribution. Therefore, in this paper, we proposed a time–frequency representation method based on sparse representation and WVD. Unlike the traditional kernel function methods to suppress cross terms, the proposed method not only reduces the interfering cross terms but also preserves the superb time–frequency concentration of the WVD.

Each atom in the dictionary has its time–frequency characteristics as shown in Fig. 8, and the WVD of the  $i$ th atom is defined as

$$\mathbf{W}_{\text{atom}(i)}(t, f) = \int_{-\infty}^{\infty} g_{(i)}\left(t + \frac{\tau}{2}\right) g_{(i)}^*\left(t - \frac{\tau}{2}\right) e^{-j2\pi f t}. \quad (19)$$

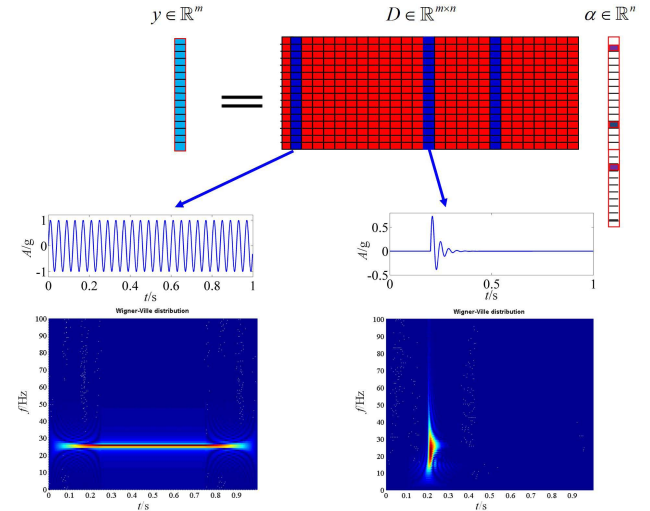


Fig. 8. STFR of each atom.

Then, the STFR of the whole signal  $s$  can be implemented by integrating the time–frequency distribution characteristics of the atoms with nonzero coefficients and corresponding sparse coefficients

$$\mathbf{STF}_s = \sum_{i=1}^N \hat{x}_i \mathbf{W}_{\text{atom}(i)} \quad (20)$$

where  $\mathbf{W}_{\text{atom}(i)}$  is the WVD of the  $i$ th atom.

The proposed method implements fault diagnosis by observing if there is a fault characteristic frequency in time–frequency representation. The computational burden of the proposed method is mainly focused on solving BP algorithm. The computation complexity is  $cNIn(N)$ , where  $c$  is the number of atoms in dictionary and  $N$  is the number of points in signal. Therefore, the calculating efficiency is too low to implement real-time detection. In practical engineering, fault diagnosis of WT mainly includes condition monitoring and fault detection. Statistical indicators, such as rms and kurtosis, are currently used for condition monitoring. If the statistical indicators exceed the standard, then the proposed method can be used for analysis and precise diagnosis. And the proposed method can also be used for double-fed WT, but the parameters of dictionary should be adjusted.

## IV. SIMULATION STUDY

To verify the effectiveness of the STFR method, a simulation experiment is conducted. In this section, based on the characteristics of the WT vibration signal, a compound signal is constructed with three components and defined as

$$y(t) = s_1(t) + s_2(t) + s_3(t) \quad (21)$$

where  $s_1(t)$  is the pure sinusoid to simulate the power frequency component, i.e., the first harmonic signal.  $s_2(t)$  is the steady modulation signal and  $s_3(t)$  is the pulsing

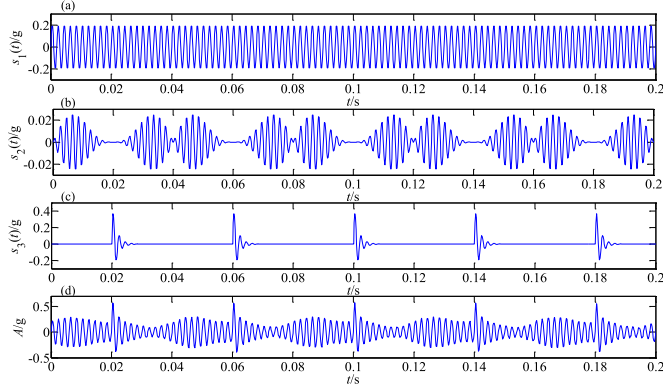


Fig. 9. Waveform of (a) harmonic component  $s_1$ , (b) steady modulation component  $s_2$ , (c) pulsing modulation component  $s_3$ , and (d) mixed signal  $y$ .

modulation signal. They are defined as

$$\begin{aligned} s_1(t) &= A_1 \sin(2\pi f_z t) \\ s_2(t) &= A_2 [\sin(2\pi f_r t) + \sin(2\pi \cdot 2f_r t)] * s_1(t) \\ s_3(t) &= X A_3 s_p(t - T_0 - [t/T] \times T) \end{aligned} \quad (22)$$

where  $A_1 = 0.2$ ,  $A_2 = 0.08$ , and  $A_3 = 0.5$  are the amplitudes of  $s_1(t)$ ,  $s_2(t)$ , and  $s_3(t)$ , respectively.  $f_z = 500$  Hz is the parameter used to simulate the stiffness fluctuation frequency.  $f_r = 25$  Hz is used to simulate the rotating frequency.  $T_0$  is the start time of the pulse signal.  $T$  is the oscillating period of  $s_p(t')$ .  $s_p(t')$  is the oscillate damping function, which is defined as

$$s_p(t') = \begin{cases} \exp \left[ \left( -\frac{\xi_1}{\sqrt{(1-2\xi_1^2)}} 2\pi f_1 t' \right) \cdot \sin(2\pi f_1 t') \right], & t' \geq 0; \\ 0, & t' < 0. \end{cases} \quad (23)$$

Let  $T_0 = 0.005$  s and  $T = 0.02$  s.  $\xi_1 = 0.2$  is the attenuation factor.  $f_1 = 500$  Hz is the carrier frequency. The waveforms of these three components and the whole signal are shown in Fig. 9.

The Fourier subdictionary is constructed with parameters  $f$ , which ranges from 0 to half of the maximum sample frequency  $f_s$ . In this simulation,  $f_s = 5000$  Hz. The Laplace wavelet subdictionary is constructed with parameters  $\tau \in [0 : 5/f_s : 0.2]$ ,  $\xi \in [0.1 : 0.01 : 0.3]$ , and  $f = 500$  Hz.

The STFR result of the compound signal is displayed in Fig. 10. Wavelet transform is always an effective method for signal analysis [34]. For the purpose of comparison, the same simulation signal is analyzed by continuous wavelet transform (CWT) with the Morlet. The CWT of a function  $x(t)$  is expressed as

$$W_x(a, b; \psi) = \int x(t) \psi_{a,b}(t) dt, a > 0 \quad (24)$$

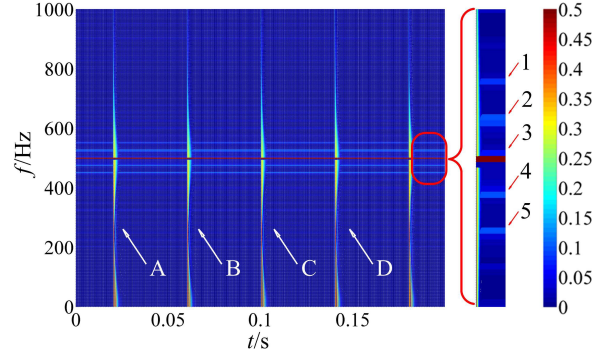


Fig. 10. STFR of the mixed signal  $y$ .

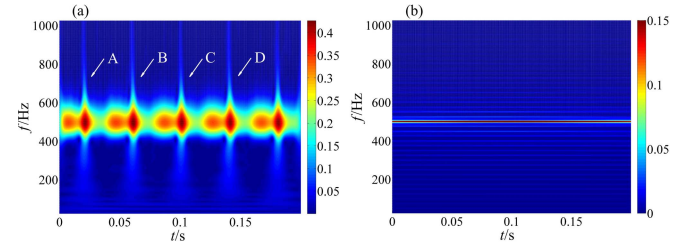


Fig. 11. Time-frequency representation of  $y$  based on Morlet wavelet with mother wavelet length of (a) 16 and (b) 256.

where the function family  $\psi_{a,b}(t)$  is generated by stretching and translating the mother wavelet  $\psi(t)$  as follows:

$$\psi_{a,b}(t) = a^{1/2} \psi \left( \frac{t-b}{a} \right) \quad (25)$$

where  $a$  is the scale factor.  $b$  is the translational value. The wavelet analysis results with the mother wavelet length of 16 and 256 are shown in Fig. 11.

It can be seen in Fig. 10 that A, B, C, and D demonstrate the periodic impact component with period of 0.04 s clearly. Furthermore, 3 demonstrates the harmonic component. 1, 2, 4, and 5 demonstrate the steady modulation component with modulation frequency of 25 Hz, which can be seen easily and matches with the constructed simulation signals accurately. Fig. 11(a) shows the periodic impact components of A, B, C, and D from the result of wavelet analysis when the wavelet length is short. And from Fig. 11(b), the harmonic component and steady modulation component can be found when wavelet length is long, but it is not as clear as in Fig. 10. However, in low-frequency band, the wavelet transform has high frequency resolution, with low time resolution, vice versa. Therefore, the analysis results are depending on the selection of wavelet length. As a result, the periodic impact can be found in Fig. 11(a) with high time resolution, while the harmonic and steady modulation components are not shown. Similarly, it can be found in Fig. 11(b), with high frequency resolution, the impact component cannot be found due to the low time resolution.

Totally with the actual situation, the simulation signal  $y$  is added with noise component

$$s(t) = y(t) + n(t) = s_1(t) + s_2(t) + s_3(t) + n(t) \quad (26)$$

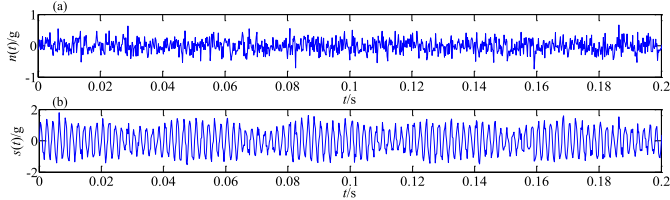


Fig. 12. Waveform of (a) noise  $n(t)$  and (b) mixed simulated signal  $s$ .

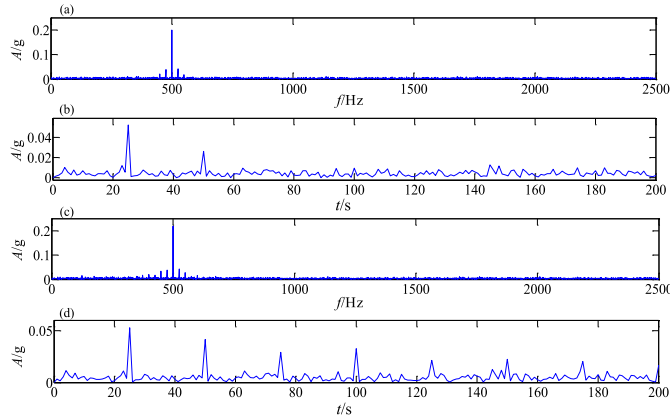


Fig. 13. (a) Envelop spectrum of  $s_1(t) + s_2(t) + n(t)$  and (b) its spectrum. (c) Envelop spectrum of  $s(t)$  and (d) its spectrum.

where  $n$  is the Gaussian white noise with zero mean and 0.15 standard deviation, as shown in Fig. 12(a). Fig. 12(b) shows the total simulated signal  $s$  with noise.

In this simulation, the envelop spectrum and frequency spectrum of  $s_1(t) + s_2(t) + n(t)$  and  $s$  are drawn in Fig. 13. It can be seen that the sideband and characteristic frequency can be seen in both the two simulated signals. Neither the envelop spectrum nor the frequency spectrum can identify the existence of pulsing modulation component  $s_3$ .

The STFR result of signal  $s$  is displayed in Fig. 14. The wavelet analysis results with the wavelet length of 16 and 256 are shown in Fig. 15.

As shown in Fig. 14, even in noisy environment, the periodic impact component with period of 0.04 s still can be found, as well as the harmonic and steady modulation components with modulation frequency of 25 Hz. However, in Fig. 15(a), only some cluttered impact can be found without regular period due to the effect of noise. In Fig. 15(b), the harmonic component and steady modulation component are still can be seen unclearly. Therefore, the STFR method not only provides a denoising algorithm for nonstationary complex signal with multicomponent coupling effect but also eliminates the cross-term interference of WVD.

To better illustrate the effectiveness of the proposed method, the time–frequency concentration measurement (CM) of each simulation is calculated as the numerical results. CM is the proportion of time–frequency energy in  $R$  set and the total time–frequency energy, which can reflect the accuracy of feature extraction by the proposed method. The results are shown in Table I.

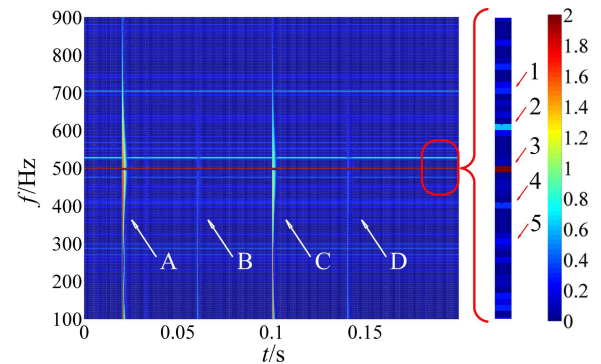


Fig. 14. STFR of the mixed signal  $s$ .

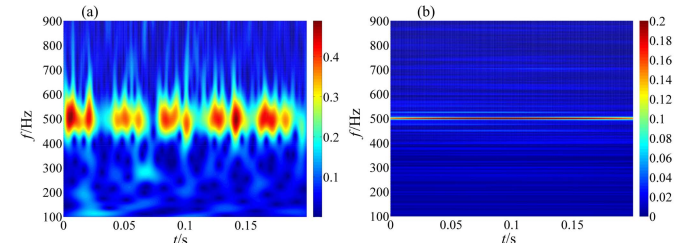


Fig. 15. Time–frequency representation of  $s$  based on Morlet wavelet with mother wavelet length of (a) 16 and (b) 256.

TABLE I  
CM RESULTS OF THE TWO SIMULATIONS

	CM of STFR	CM of wavelet transform
Noise-free simulation	1	0.4952
Noised simulation	0.9957	0.3386

Therefore, the proposed method performs better in feature extraction, and shows excellent time–frequency concentration ability.

## V. ENGINEERING APPLICATIONS

To examine the performance of the STFR method, the applications to two field tests are performed for the WT drive train incipient fault diagnosis.

### A. STFR for Gearbox

In this section, a field test of WT gearbox was used to prove the validity of the theoretical analysis and the ability for incipient fault diagnosis. To further demonstrate the effectiveness of the STFR method, the analysis result is compared with the analysis results of wavelet transform and BP sparse representation method.

This field test was performed in the WT of the WD50/800 type, with rated wind speed of 14 m/s and power of 750 kW. The diagnostic system concludes seven vibration acceleration sensors, a proximity switch for the rotational speed test, an offline data acquisition device, and a personal computer [35]. There are one low-speed planetary stage and two parallel stages in the gearbox, which has an overall ratio

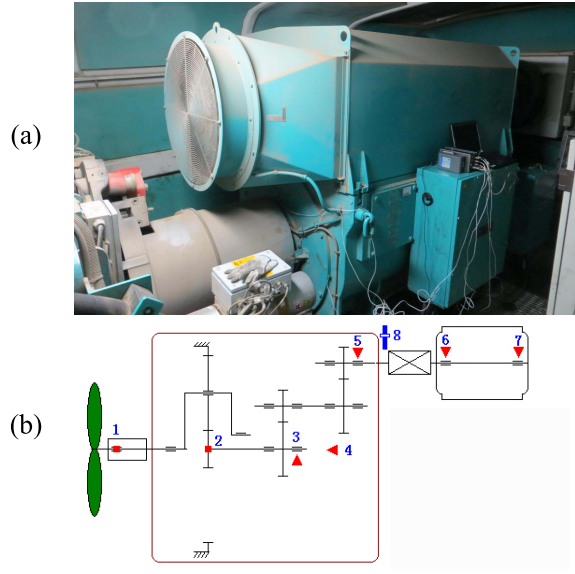


Fig. 16. (a) Overall view of WT. (b) Drivetrain configuration of the WT and gearbox transmission layout.

TABLE II  
SENSORS TYPES AND THE NAMES OF MEASUREMENT POINTS

No.	Name of measure point
1	Horizontal direction of main shaft bearing
2	Horizontal direction of gear ring of planetary gearbox
3	Vertical direction of output shaft of planetary gearbox
4	Horizontal direction of output shaft of planetary gearbox
5	Vertical direction of output shaft of parallel shaft gearbox
6	Vertical direction of input shaft of generator
7	Vertical direction of output shaft of generator
8	Output shaft of gearbox

TABLE III  
BASIC KINEMATIC DATA OF THE GEARBOX UNDER CONSIDERATION

Parameters	Relative frequency	Frequency (Hz)
Generator shaft	1	25
Intermediate shaft	0.2794	6.9853
Sun shaft	0.0733	1.8325
Planets	0.0444	1.1098
Main rotor	0.0148	0.3699
Meshing parallel gear I	19	475
Meshing parallel gear II	5.8677	146.691
Meshing parallel gear	1.3466	33.665

of 1:61.713. The drive train configuration and the transmission layout of the gearbox are presented in Fig. 16. Points 1–7 in Fig. 16(b) are the locations of vibration acceleration sensors in the WT, and point 8 is the location of a laser displacement sensor to measure the rotating speed. The sensors types and the names of measure points are displayed in Table II. Table III presents the basic characteristic frequencies. Relative frequencies in Table III are related to the generator shaft frequency. The running speed of the generator was 1500 rpm, for which vibration signals were collected from sensor 5 with the sampling frequency 25.6 kHz.

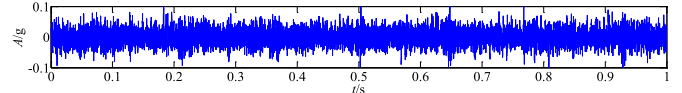


Fig. 17. Vibration signal of the WT gearbox.

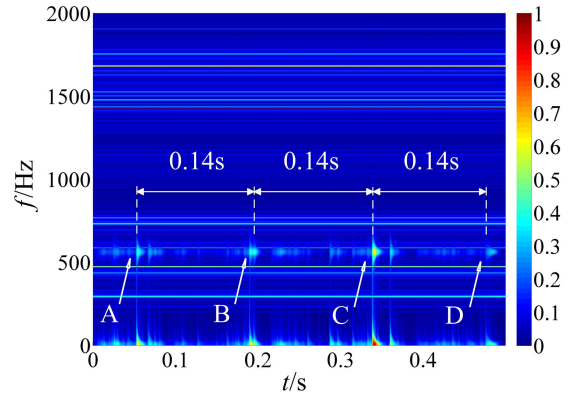


Fig. 18. STFR result of the vibration signal.

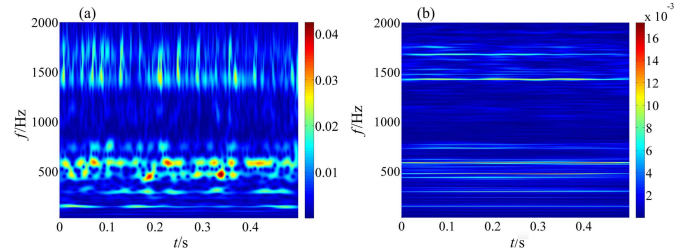


Fig. 19. Time-frequency representation of the vibration signal via wavelet transform with mother wavelet length of (a) 16 and (b) 256.

One segment time-domain signal of the vibration signal with a time length of 0.5 s is shown in Fig. 17. As can be seen, there is no significant information for fault diagnosis.

To decrease the computation cost, the vibration signal is preprocessed by four times down sampling. The STFR method with the URD is then applied for vibration signal processing. The URD is constructed with the parameters  $\tau \in [0 : 5/f_s : 0.5]$ ,  $\xi \in [0.05 : 0.01 : 0.2]$ , and  $f = 590$  Hz. The STFR result is displayed in Fig. 18. The same vibration signal is processed by the wavelet transform and Hamming window. The results are shown in Figs. 19 and 20. The change in the wavelet scale is due to different methods used in Figs. 19 and 20; therefore, there is no reason to keep the window length the same. We chose the best results for display in this paper, instead of the results with the same window length.

On one hand, as shown in Fig. 18, the steady meshing frequencies and corresponding harmonics can be found clearly. Furthermore, the periodic impact components A, B, C, and D with interval of 0.14 s are also illustrated in Fig. 18, which accurately matches with the rotation period of intermediate shaft 1/6.9853 as shown in Table III. Therefore, based on the STFR result, it can be concluded that there may be a localized fault in intermediate shaft.

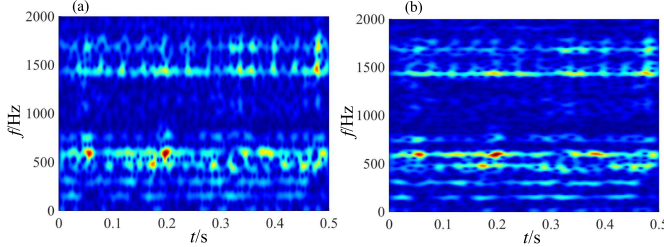


Fig. 20. Sparse time–frequency transform (STFT) result of Hamming window with the window function length of (a) 64 and (b) 128.

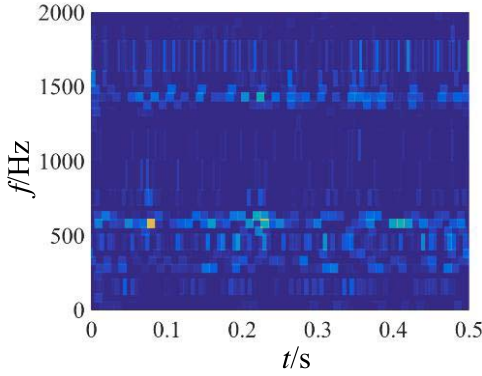


Fig. 21. Analyze result of BP method in [30].



Fig. 22. Spalls on the gear of the intermediate shaft.

On the other hand, the results of wavelet transform fail to reflect in the operation condition of the gearbox as shown in Fig. 19. Fig. 19(a) shows some messy impacts when the wavelet is short, but without obvious period. In Fig. 19(b), the meshing frequencies can be found when wavelet is long. However, this information is not enough to diagnose the fault. It can also be found in Fig. 20 that impact components can hardly be found in the result of Hamming window for gearbox.

Since the proposed method is a time–frequency decomposition technique, another comparison with BP sparse decomposition method proposed in [30] is also conducted to verify its advantages in time–frequency decomposition. The dictionary is constructed as wavelet packet dictionary. The analyzed result is shown in Fig. 21.

It can be seen from Fig. 21 that the impact vibration component for fault prognosis can be hardly distinguished under the high harmonic vibration interference.

TABLE IV  
PARAMETERS OF THE BEARING

Positions	Characteristic frequency/Hz	Frequency /Hz
Outer race	78.3171	3.1327
Inner race	121.683	4.8673
Rolling element	109.877	4.3951
Cage	9.7896	0.3916

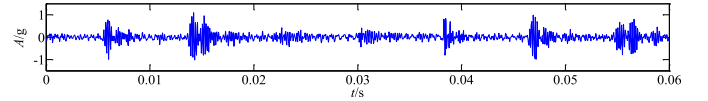


Fig. 23. Vibration signal of the WT generator.

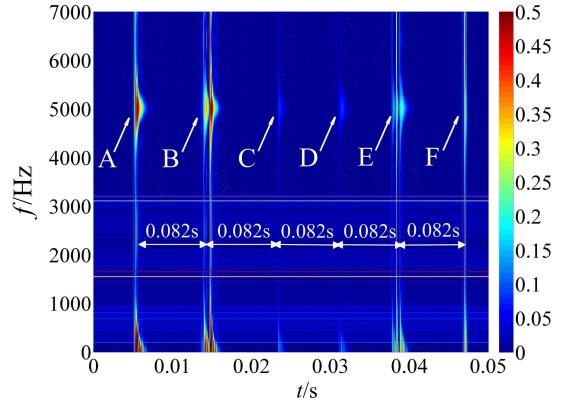


Fig. 24. STFR result of the vibration signal.

Then, endoscopy was performed to detect the gearbox. And a slight localized fault, spalling, was found on the gear wheel of the intermediate shaft, as shown in Fig. 22, which is same as the STFR result.

#### B. STFR for Bearing in WT Generator

In this section, another field test was performed to demonstrate the effectiveness of the proposed method. The WT is of the WD50/800 type, which the drivetrain configuration and the transmission layout are the same as in last test shown in Fig. 16. In this test, vibration signals were collected from sensor 6 with the sampling frequency 25.6 kHz. Therefore, the vibration signal collected reflects the condition of generator. The bearing is of SKF 6326c3 type. The parameters of the bearing are listed in Table IV. The values of characteristic frequencies are under the rotation speed of 1500 rpm.

One segment time-domain signal of the vibration signal with a time length of 1 s is shown in Fig. 23. It can be seen that the condition can be hardly displayed by the signal.

The URD is constructed with the parameters  $\tau \in [0 : 5/f_s : 0.06]$ ,  $\zeta \in [0.05 : 0.01 : 0.2]$ , and  $f = 5000$  Hz. Then, the STFR method is applied for the WT incipient fault diagnosis over the URD, and the result is shown in Fig. 24. The same vibration signal is processed using the Morlet wavelet transform and Hamming window. The results are shown in Figs. 25 and 26.

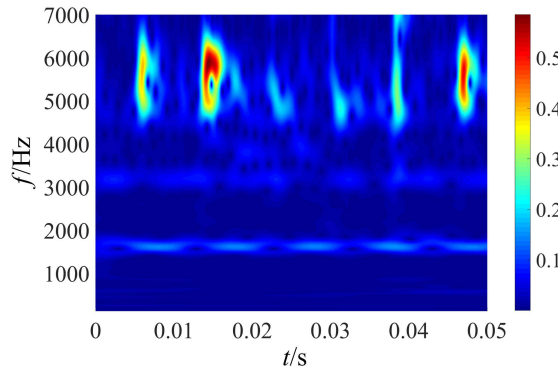


Fig. 25. Time–frequency representation of the vibration signal via wavelet transform.

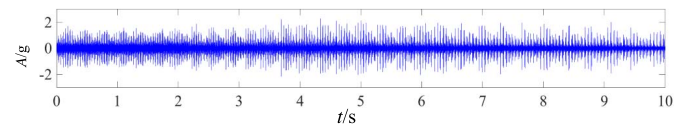


Fig. 27. Vibration signal with a time length of 10 s under variable speed.

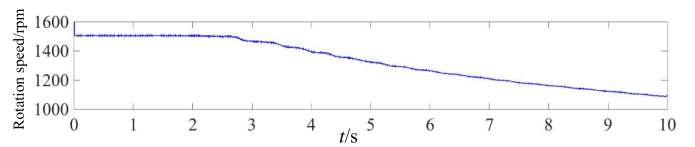


Fig. 28. Corresponding rotation speed.

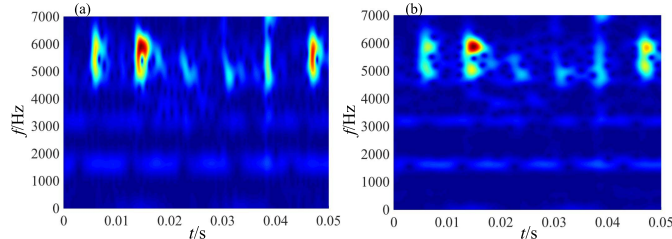


Fig. 26. STFT result of Hamming window with the window function length of (a) 64 and (b).

It can be seen in Fig. 24 that both the harmonic steady modulation and impact components can be found from the STFR. Furthermore, the impact components are illustrated by A, B, C, D, E, and F with the duration of 0.082 s, which matches with the rotation period of inner race 1/121.683 as shown in Table III. The STFR result indicates that there is a localized fault on the inner race of the generator bearing. By the way of comparison in Figs. 25 and 26, there are some impacts that can be found in the results of wavelet transform and Hamming window, but it is too ambiguous to conclude that there is a fault.

Since the rotation speed fluctuation will lead to the fluctuation of instantaneous frequency of stationary component, but will not influence the form of impact component, because the impact component only depends on the inherent property of mechanical system. Therefore, the speed fluctuation will affect the extraction of stationary component of the proposed method, but will not influence the extraction of impact component. And the local fault can still be diagnosed by observing if there is an impact vibration component related with rotating speed existed in the time–frequency representation.

To verify the advantages of the proposed method in dealing with nonstationary signals, the proposed method is used to analyze the vibration signals of the same bearing under variable speed operational condition. The vibration signal with a time length of 10 s is shown in Fig. 27. The corresponding rotation speed is shown in Fig. 28.

The signal between 4 and 4.05 s is intercepted for analysis, and the analyze result is shown in Fig. 29.

It can be seen that the impact component can still be extracted; therefore, the local fault can also be diagnosed.

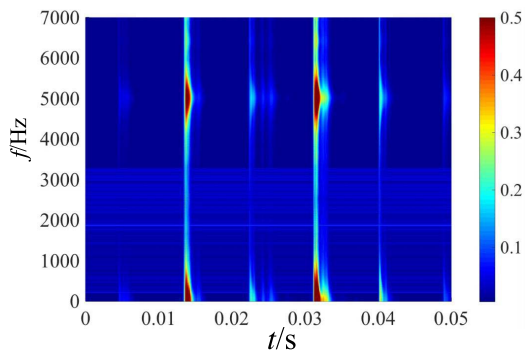


Fig. 29. STFR result of the vibration signal under variable speed operational condition.

Therefore, the experiment results illustrate the effectiveness of the STFR method for incipient fault diagnosis of WT drive train and damage location. Furthermore, it can also overcome the limitations of traditional wavelet transform methods.

## VI. CONCLUSION

The STFR method based on sparse representation theory and WVD is proposed in this paper for WT drive train incipient fault diagnosis. The URD applied in this method is constructed based on the prior knowledge of vibration signal model. It is composed of Fourier subdictionary and Laplace subdictionary, which is similar with the inner structure of vibration signal components. The sparse coefficients can be obtained by solving the BPDN problem based on the constructed dictionary, which shows the superior noise reduction ability and, furthermore, retains the time–frequency energy concentration. Compared with traditional WVD, the STFR method solves the interference of cross term in WVD, which is a benefit for fault feature information extraction. It can be found from the results of simulation and experiments that the condition information and even the fault location are shown clearly in the result of STFR. And this illustrates the effectiveness and the robustness of the STFR method in the engineering applications with strong noise and multicomponent coupling effect.

## REFERENCES

- [1] A. Kaabeche, M. Belhamel, and R. Ibtouen, "Sizing optimization of grid-independent hybrid photovoltaic/wind power generation system," *Energy*, vol. 36, no. 2, pp. 1214–1222, 2011.
- [2] A. Cavallo, "Controllable and affordable utility-scale electricity from intermittent wind resources and compressed air energy storage (CAES)," *Energy*, vol. 32, no. 2, pp. 120–127, 2007.
- [3] M. Z. Jacobson, "Review of solutions to global warming, air pollution, and energy security," *Energy Environ. Sci.*, vol. 2, no. 2, pp. 148–173, 2009.
- [4] J.-M. Muñoz-Ferreras, Z. Peng, Y. Tang, R. Gómez-García, D. Liang, and C. Li, "Short-range Doppler-radar signatures from industrial wind turbines: Theory, simulations, and measurements," *IEEE Trans. Instrum. Meas.*, vol. 65, no. 9, pp. 2108–2119, Sep. 2016.
- [5] S. Sawyer and K. Rave, "Global wind report," in *Global Wind Energy Council (GWEC)*, 2014.
- [6] F. Blaabjerg and K. Ma, "Future on power electronics for wind turbine systems," *IEEE J. Emerg. Sel. Topics Power Electron.*, vol. 1, no. 3, pp. 139–152, Sep. 2013.
- [7] J. Igba, K. Alemzadeh, C. Durugbo, and K. Henningsen, "Performance assessment of wind turbine gearboxes using in-service data: Current approaches and future trends," *Renew. Sustain. Energy Rev.*, vol. 50, pp. 144–159, Oct. 2015.
- [8] W. Qiao and D. Lu, "A survey on wind turbine condition monitoring and fault diagnosis—Part I: Components and subsystems," *IEEE Trans. Ind. Electron.*, vol. 62, no. 10, pp. 6536–6545, Oct. 2015.
- [9] P. Tavner, "How are we going to make offshore wind farms more reliable?" *Supergen Wind*, 2011.
- [10] J. Gallego-Calderon and A. Natarajan, "Assessment of wind turbine drive-train fatigue loads under torsional excitation," *Eng. Struct.*, vol. 103, pp. 189–202, Nov. 2015.
- [11] J. G. Holierhoek, "Procedures for testing and measuring wind turbine components; results for yaw and pitch system and drive train," *Wind Energy*, vol. 16, no. 6, pp. 827–843, 2013.
- [12] F. Miao, H. Shi, and X. Zhang, "Impact of the converter control strategies on the drive train of wind turbine during voltage dips," *Energies*, vol. 8, no. 10, pp. 11452–11469, 2015.
- [13] R. Liu, G. Meng, B. Yang, C. Sun, and X. Chen, "Dislocated time series convolutional neural architecture: An intelligent fault diagnosis approach for electric machine," *IEEE Trans. Ind. Inf.*, vol. 13, no. 3, pp. 1310–1320, Jun. 2017.
- [14] A. Kusiak, Z. Zhang, and A. Verma, "Prediction, operations, and condition monitoring in wind energy," *Energy*, vol. 60, pp. 1–12, Oct. 2013.
- [15] K.-Y. Oh, J.-Y. Park, J.-S. Lee, B. I. Epureanu, and J.-K. Lee, "A novel method and its field tests for monitoring and diagnosing blade health for wind turbines," *IEEE Trans. Instrum. Meas.*, vol. 64, no. 6, pp. 1726–1733, Jun. 2015.
- [16] N. E. Huang *et al.*, "The empirical mode decomposition and the Hilbert spectrum for nonlinear and non-stationary time series analysis," *Proc. Roy. Soc. London Ser. A, Math., Phys. Eng. Sci.*, vol. 454, no. 1971, pp. 903–995, Mar. 1998.
- [17] R. Yan, R. X. Gao, and X. Chen, "Wavelets for fault diagnosis of rotary machines: A review with applications," *Signal Process.*, vol. 96, pp. 1–15, Mar. 2014.
- [18] M. S. Manikandan, S. R. Samantaray, and I. Kamwa, "Detection and classification of power quality disturbances using sparse signal decomposition on hybrid dictionaries," *IEEE Trans. Instrum. Meas.*, vol. 64, no. 1, pp. 27–38, Jan. 2015.
- [19] B. Chen, Z. Zhang, C. Sun, B. Li, Y. Zi, and Z. He, "Fault feature extraction of gearbox by using overcomplete rational dilation discrete wavelet transform on signals measured from vibration sensors," *Mech. Syst. Signal Process.*, vol. 33, pp. 275–298, Nov. 2012.
- [20] Y. Wang, Z. He, and Y. Zi, "A comparative study on the local mean decomposition and empirical mode decomposition and their applications to rotating machinery health diagnosis," *J. Vibrat. Acoust.*, vol. 132, no. 2, p. 021010, Mar. 2010.
- [21] R. Li and D. He, "Rotational machine health monitoring and fault detection using EMD-based acoustic emission feature quantification," *IEEE Trans. Instrum. Meas.*, vol. 61, no. 4, pp. 990–1001, Apr. 2012.
- [22] J. Antoni, "Fast computation of the kurtogram for the detection of transient faults," *Mech. Syst. Signal Process.*, vol. 21, no. 1, pp. 108–124, 2007.
- [23] B. Yang, R. Liu, and X. Chen, "Fault diagnosis for a wind turbine generator bearing via sparse representation and shift-invariant K-SVD," *IEEE Trans. Ind. Informat.*, vol. 13, no. 3, pp. 1321–1331, Jun. 2017.
- [24] E. J. Candès, J. K. Romberg, and T. Tao, "Stable signal recovery from incomplete and inaccurate measurements," *Commun. Pure Appl. Math.*, vol. 59, no. 8, pp. 1207–1223, 2006.
- [25] H. Liu, S. Li, and L. Fang, "Robust object tracking based on principal component analysis and local sparse representation," *IEEE Trans. Instrum. Meas.*, vol. 64, no. 11, pp. 2863–2875, Nov. 2015.
- [26] S. Li and L. Fang, "Signal denoising with random refined orthogonal matching pursuit," *IEEE Trans. Instrum. Meas.*, vol. 61, no. 1, pp. 26–34, Jan. 2012.
- [27] L. Fang and S. Li, "Face recognition by exploiting local Gabor features with multitask adaptive sparse representation," *IEEE Trans. Instrum. Meas.*, vol. 64, no. 10, pp. 2605–2615, Oct. 2015.
- [28] S. G. Mallat and Z. Zhang, "Matching pursuits with time-frequency dictionaries," *IEEE Trans. Signal Process.*, vol. 41, no. 12, pp. 3397–3415, Dec. 1993.
- [29] S. S. Chen, D. L. Donoho, and M. A. Saunders, "Atomic decomposition by basis pursuit," *SIAM Rev.*, vol. 43, no. 1, pp. 129–159, 2001.
- [30] H. Yang, J. Mathew, and L. Ma, "Fault diagnosis of rolling element bearings using basis pursuit," *Mech. Syst. Signal Process.*, vol. 19, no. 2, pp. 341–356, Mar. 2005.
- [31] S. Boyd, N. Parikh, E. Chu, B. Peleato, and J. Eckstein, "Distributed optimization and statistical learning via the alternating direction method of multipliers," *Found. Trends Mach. Learn.*, vol. 3, no. 1, pp. 1–122, Jan. 2011.
- [32] R. F. Orsagh, H. Lee, M. Watson, C. S. Byington, and J. Powers, "Advanced vibration monitoring for wind turbine health management," in *Impact Technologies*. 2006. [Online]. Available: <http://www.impact-tek.com>
- [33] R. Liu, B. Yang, X. Zhang, S. Wang, and X. Chen, "Time-frequency atoms-driven support vector machine method for bearings incipient fault diagnosis," *Mech. Syst. Signal Process.*, vol. 75, pp. 345–370, Jun. 2016.
- [34] A. D. Spyrosarios, M. G. Dimopoulos, and A. A. Hatzopoulos, "Wavelet analysis for the detection of parametric and catastrophic faults in mixed-signal circuits," *IEEE Trans. Instrum. Meas.*, vol. 60, no. 6, pp. 2025–2038, Jun. 2011.
- [35] J. Li, X. Chen, Z. Du, Z. Fang, and Z. He, "A new noise-controlled second-order enhanced stochastic resonance method with its application in wind turbine drivetrain fault diagnosis," *Renew. Energy*, vol. 60, pp. 7–19, Dec. 2013.



**Boyuan Yang** (GS'18) received the B.S. degree in Qian Xuesen experimental class from Xi'an Jiaotong University, Xi'an, China, in 2013, where he is currently pursuing the Ph.D. degree in mechanical engineering.

His current interests include wind turbine fault diagnostics, signal sparse representation and time-frequency representation, data-driven prognostics, and health management.



**Ruonan Liu** received the B.S. degree from Xi'an Jiaotong University, Xi'an, China, in 2013, where she is currently pursuing the Ph.D. degree in mechanical engineering.

Her current research interests include machine learning, deep learning, and sparse signal representation for mechanical signal processing, and diagnosis and prognosis for industrial systems.



**Xuefeng Chen** received the Ph.D. degree from Xi'an Jiaotong University, Xi'an, China, 2004.

He is currently a Professor of mechanical engineering with Xi'an Jiaotong University. His current research interests include finite-element method, machinery condition monitoring, and prognostics.

Dr. Chen was a recipient of the National Excellent Doctoral Dissertation of China in 2007, the Second Awards of Technology Invention of China in 2009, and the National Science Fund for Distinguished Young Scholars in 2012.